Journal of Sound and Vibration (2002) **254**(5), 939–949
doi:10.1006/jsvi.2001.4138, available online at http://www.idealibrary.com on IDEAL®

NATURAL FREQUENCIES AND MODE SHAPES OF A FREE–FREE BEAM WITH LARGE END MASSES

C. L. Kirk and S. M. Wiedemann

College of Aeronautics, Cranfield University, Cranfield, Bedford MK43 0AL, England

(*Received* 6 *April* 2001, *and in final form* 10 *October* 2001)

An analytical solution is presented for the natural frequencies, mode shapes and orthogonality condition, of a free–free beam with large off-set masses connected to the beam by torsion springs. Results are given for a range of masses with various fixed orientations and the validity of the method is confirmed against established results for natural frequencies of beams with five different boundary conditions. The study lays the foundation for investigations into the dynamics and vibration control of multi-link articulated systems such as the Space Shuttle Remote Manipulator.

1. INTRODUCTION

In recent years considerable interest has been shown in the vibration and control of flexible beams subject to rotational manoeuvres due to torque motors, producing acceleration/deceleration sequences. Of particular interest is the effect of flexibility in robot arms, for example, the Space Shuttle Remote Manipulator System (SRMS) and the Space Station Mobile Manipulator System (MMS). These robots have basically two articulated flexible links with various rotational degrees of freedom about the revolute joints.

Dynamic analysis of such systems has generally been carried out by assuming approximate mode shapes for the separate links (for example reference [1]), taken as mode shapes for uniform beams without end masses or rotary inertias. A literature search shows that this approach has not been verified by comparison with the exact solution based on the classical Bernoulli beam theory.

This paper presents an exact solution for the natural frequencies and mode shapes of the lower modes, of a single link with overhanging end masses and rotary inertias as shown in Figure 1, as a prelude to studying the vibration of two-link articulated systems, such as used in the SRMS. The analysis also includes torsion springs between the masses and the ends of the beam to simulate joint flexibility.

Many authors have studied the effect of concentrated masses and springs on beam natural frequencies with approximate or exact analytical methods but have rarely included the mode shapes [2–10]. Few authors have considered the present problem of solving the beam differential equation (1) with the boundary conditions relevant to Figure 1.

However, the authors of references [11, 12] have studied a similar problem for a ground-based-single-link flexible robot, but with one end inertially pinned. An approximate solution to a two-link Space Shuttle Manipulator was studied in reference [13] with torsion spring restrained joints and fixed link configurations, for the first four natural frequencies of the Shuttle–payload system.

0022-460X/02/$35.00

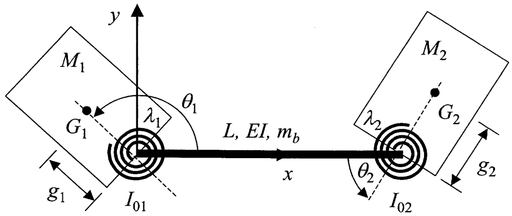

Figure 1. Free–free beam with end masses and torsion springs.

2. NATURAL FREQUENCY AND MODE SHAPE DETERMINATION

The free–free beam system is shown in Figure 1, with end masses M_i and rotary inertias I_{0i} about the ends of the beam. G_i are the centres of masses, λ_i the torsional springs stiffnesses, and EI, m_b and L the usual notation for the uniform beam.

The angles θ_i are constant for the undeformed system. Neglecting rotary inertia and shear, the equation of beam vibration is [14]

$$EI\ y^{\mathrm{iv}}(x,t) + m_b\,\ddot{y}(x,t) = 0. \tag{1}$$

Using the method of separation of variables the solution to equation (1) yields the eigenfunctions for the nth mode shape as

$$y_n(x) = A\sin(kx) + B\cos(kx) + C\sinh(kx) + D\cosh(kx), \tag{2}$$

where

$$k^2 = \omega_n\sqrt{\frac{m_b}{EI}} \tag{3}$$

and ω_n is the nth natural frequency.

The arbitrary constants are eliminated from equation (2) by means of the four boundary conditions at $x = 0$ and L.

Figure 2 shows the boundary condition geometry at $x = 0$, where $y(0)$ is the deflection and $y'(0)$ the slope of the beam, and θ_1 the fixed angle between O_1G_1 and the undeformed beam axis. Angle α_1 is the rotation of the mass relative to the beam due to the torsion spring of stiffness λ_1.

Since the springs are placed between the beam and the masses, moment equilibrium gives

$$\alpha_1 = \frac{EI\,y''(0)}{\lambda_1}, \qquad \alpha_2 = \frac{EI\,y''(L)}{\lambda_2}. \tag{4a, 4b}$$

Bending moment equilibrium: At $x = 0$, the mass centre G_1 has an acceleration $\ddot{u} = -\,y(0)\omega^2$ perpendicular to the beam. Thus, the moment about O_1 due to this acceleration is $-M_1 g_1\omega^2\ y(0)\cos\theta_1$. Similarly the rotary inertia of the mass produces a moment about O_1 which is equal to $-\,I_{01}\omega^2[y'(0) - \alpha_1]$. Hence,

$$EI\ y''(0) = -\,I_{01}\omega^2[y'(0) - \alpha_1] - g_1 M_1\omega^2[y(0)\cos\theta_1]. \tag{5}$$

Shear force equilibrium: The total acceleration of G_1 is due to the transverse acceleration $\omega^2 y(0)$ and the rotational acceleration $g_1[y'(0) - \alpha_1]\omega^2$. Hence, resolving the second term

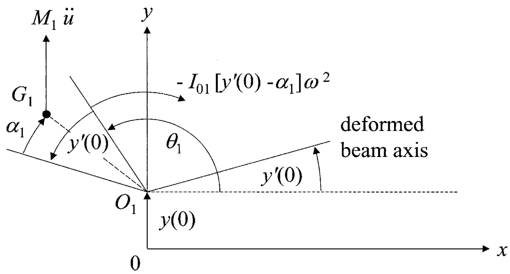

Figure 2. Boundary conditions at $x = 0$.

perpendicular to the beam, the total shear force is

$$EI\, y'''(0) = M_1\omega^2 y(0) + g_1 M_1\omega^2[y'(0) - \alpha_1]\cos\theta_1. \tag{6}$$

Similarly at $x = L$, bending moment and shear force equilibrium is

$$EI y''(L) = I_{02}\omega^2[y'(L) - \alpha_2] + g_2 M_2\omega^2[y(L)\cos\theta_2], \tag{7}$$

$$EI y'''(L) = -\, M_2\omega^2 y(L) - g_2 M_2\omega^2[y'(L) - \alpha_2]\cos\theta_2. \tag{8}$$

In the foregoing analysis, it is assumed that the angular rotations α_i and $y'(x)$ are small compared with the fixed angles θ_i, which can therefore be assumed constant during vibration.

Substituting into equations (5)–(8), the various derivatives of equation (2) and including equations (4) gives

$$\begin{bmatrix} d_{11} & d_{12} & d_{13} & d_{14} \\ d_{21} & d_{22} & d_{23} & d_{24} \\ d_{31} & d_{32} & d_{33} & d_{34} \\ d_{41} & d_{42} & d_{43} & d_{44} \end{bmatrix} \begin{bmatrix} A \\ B \\ C \\ D \end{bmatrix} = \mathbf{0} \tag{9}$$

and since A–D are generally non-zero, equation (9) only has a solution if

$$\det[d_{ij}] = \mathbf{0}. \tag{10}$$

Implementation of the above procedure is excessively tedious and resort to computer evaluation is made and programmes with the ability to handle symbolic calculations such as MATLAB or MATHEMATICA are appropriate.

Using the notation $C = \cos(kL)$, $S = \sin(kL)$, $Ch = \cosh(kL)$ and $Sh = \sinh(kL)$ results in the following expressions for the d_{ij}:

$$d_{11} = d_{13} = I_{01}k\omega^2,$$

$$d_{12} = -EI\,k^2 + \frac{EI\,I_1 k^2\omega^2}{\lambda_1} + g_1 M_1\omega^2\left[\frac{EI\,g_1 k^2}{\lambda_1} + \cos\theta_1\right],$$

$$d_{14} = EI\,k^2 - \frac{EI\,I_1 k^2 \omega^2}{\lambda_1} + g_1 M_1 \omega^2 \left[-\frac{EI\,g_1 k^2}{\lambda_1} + \cos\theta_1 \right],$$

$$d_{21} = EIk^3 + g_1 k M_1 \omega^2 \cos\theta_1,$$

$$d_{22} = M_1 \omega^2 \left[1 + \frac{EI\,g_1 k^2 \cos\theta_1}{\lambda_1} \right],$$

$$d_{23} = -EI\,k^3 + g_1 k M_1 \omega^2 \cos\theta_1,$$

$$d_{24} = M_1 \omega^2 \left[1 - \frac{EI\,g_1 k^2 \cos\theta_1}{\lambda_1} \right],$$

$$d_{31} = EIk^2 S + g_2 M_2 \omega^2 \cos\theta_2\, S + I_{02} \left[kC - \frac{EIk^2 S}{\lambda_2} \right] \omega^2,$$

$$d_{32} = EIk^2 C + g_2 M_2 \omega^2 \cos\theta_2\, C - I_{02} \left[kS + \frac{EIk^2 C}{\lambda_2} \right] \omega^2,$$

$$d_{33} = g_2 M_2 \omega^2 \cos\theta_2 Sh - EIk^2 Sh + I_{02} \left[k\,Ch + \frac{EIk^2\,Sh}{\lambda_2} \right] \omega^2,$$

$$d_{34} = g_2 M_2 \omega^2 \cos\theta_2 Ch - EIk^2 Ch + I_{02} \left[k\,Sh + \frac{EIk^2\,Ch}{\lambda_2} \right] \omega^2,$$

$$d_{41} = -\,EIk^3 C + M_2 \omega^2 S + M_2 \omega^2 g_2 \cos\theta_2 \left[kC - \frac{EIk^2 S}{\lambda_2} \right],$$

$$d_{42} = EIk^3 S + M_2 \omega^2 C - M_2 \omega^2 g_2 \cos\theta_2 \left[kS + \frac{EIk^2 C}{\lambda_2} \right],$$

$$d_{43} = EIk^3 Ch + M_2 \omega^2 Sh + M_2 \omega^2 g_2 \cos\theta_2 \left[k\,Ch + \frac{EIk^2\,Sh}{\lambda_2} \right],$$

$$d_{44} = EIk^3 Sh + M_2 \omega^2 Ch + M_2 \omega^2 g_2 \cos\theta_2 \left[k\,Sh + \frac{EIk^2\,Ch}{\lambda_2} \right]. \tag{11}$$

3. NUMERICAL RESULTS

Figure 1 shows that a wide range of values for M_i, I_{0i}, θ_i and g_i are possible. For example the single link could be an approximation to the two-link Shuttle RMS, with M_1 and I_{01} being the Shuttle mass and moment of inertia about the RMS base, and M_2 and I_{02} representing the payload. Thus, the natural frequencies could be determined for fixed M_i and I_{0i}, over a range of values of θ_1 and θ_2. This would correspond to different quasi-stationary orientations of the Shuttle and payload relative to the arm during a manoeuvre of the SRMS. Also the revolute joints O_1 and O_2 could be either free or locked with fixed values of λ_i. The torsion springs represent the stiffnesses λ_i of the joints and gear teeth in the drive gear boxes when the joints are locked.

TABLE 1

Natural frequencies of beam with zero end masses [15]

	a_1	a_2	a_3	a_4
FF	22·3733	61·6728	120·9034	199·8594
PP	9·8696	39·4784	88·8264	157·9137
CC	22·3733	61·6728	120·9034	199·8594
CF	3·5160	22·3733	61·6728	120·9034
PF	15·4182	49·9649	104·2477	178·2697

First consider the validation of equation (10) using the computed ω_n for uniform beams with free–free (FF), pinned–pinned (PP), clamped–clamped (CC), clamped–free (CF) and pinned–free (PF) end conditions, by comparing with the known analytical results obtained by solving equation (1). For example [15] gives the natural frequencies.

$$\omega_n = a_n \sqrt{\frac{EI}{m_b L^4}} \tag{12}$$

where the a_n are listed in Table 1 for the above cases.

To simulate these results using equation (10) we use $\theta_1 = \theta_2 = 0$ and for the five cases the following data. Note that if the joint angles play no role, for example, when the masses are set equals to zero, λ_1 and λ_2 are set to say unity, and if pure revolute joints are needed, they are set to a very small value, say 10^{-5}, but never equal to zero as they appear in some denominators (equations (11)).

FF: $M_1 = M_2 = I_{01} = I_{02} = g_1 = g_2 = 0$, $\lambda_1 = \lambda_2 = 1$.
PP: $M_1 = M_2 = 10^{10}$, $I_{01} = I_{02} = g_1 = g_2 = 0$, $\lambda_1 = \lambda_2 = 1$.
CC: $M_1 = M_2 = I_{01} = I_{02} = 10^{15}$, $g_1 = g_2 = 0$, $\lambda_1 = \lambda_2 = 10^{15}$.
CF: $M_1 = I_{01} = 10^{15}$, $M_2 = I_{02} = g_1 = g_2 = 0$, $\lambda_1 = 10^{15}$ and $\lambda_2 = 1$.
PF: $M_1 = 10^{15}$, $M_2 = I_{01} = I_{02} = g_1 = g_2 = 0$, $\lambda_1 = \lambda_2 = 1$.

The beam properties were taken from the averaged two-link SRMS data [16] as $m_b = 3{\cdot}6$ kg/m, $EI = 3 \times 10^6$ N m^2, $L = 14$ m.

Comparison of the results from equation (10) with equation (12) gave exact agreement within the limits of numerical accuracy. Identical results were also obtained by reversing the data, writing M_2, I_{02} instead of M_1, I_{01}.

The lower natural frequencies, say ω_1 and ω_2, were examined for typical values of M_i, I_{0i}, λ_i and θ_i. Because of the almost infinite range of values just a few were selected to illustrate trends which will indicate how the ω_n depend on these parameters. This is important for dynamic response analysis where it is necessary to know, for example, how θ_1 and θ_2 influence the results. Also M_2 may be a rectangle with length $a \gg b$, with the beam attachment as shown in Figure 3 or 4 where the effect of the overhang of the mass centre G_2 and angle θ_2 are parameters of interest. For example, M_1 could be the idealized mass of the Shuttle and M_2 the idealized mass of a prismatic payload with uniform mass distribution.

For configuration (C1) in Figure 3 select, say, $M_1 = 70\,000$ kg, $M_2 = 10\,000$ kg, $I_{01} = 1{\cdot}472 \times 10^7$ kg m^2, $a = 6$ m, $b = 2$ m, hence $I_{02} = 1{\cdot}275 \times 10^5$ kg m^2, $g_1 = 14$ m,

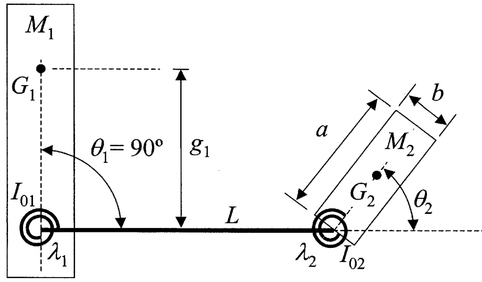

Figure 3. Configuration C1.

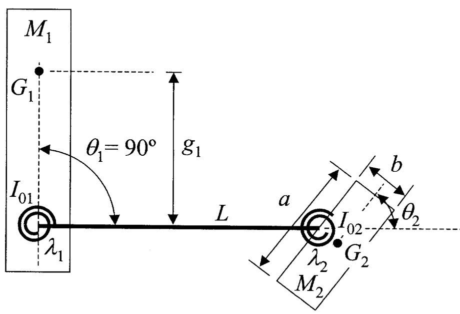

Figure 4. Configuration C2.

TABLE 2

Natural frequencies ω_1 *and* ω_2 (rad/s) *for configurations C1 and C2*

	C1		C2	
θ_2(deg)	ω_1	ω_2	ω_1	ω_2
0	0·394	4·432	0·457	3·771
10	0·395	4·270	0·457	3·752
20	0·398	3·881	0·459	3·697
30	0·402	3·431	0·461	3·614
40	0·409	3·022	0·465	3·515
50	0·417	2·686	0·469	3·410
60	0·428	2·422	0·474	3·308
70	0·441	2·219	0·480	3·217
80	0·457	2·068	0·486	3·142
90	0·475	1·959	0·493	3·084

$g_2 = 3$ m, $\lambda_1 = \lambda_2 = 10^6$ N m/rad, $m_b = 3{\cdot}6$ kg/m, $EI = 3 \times 10^6$ N m^2 and $L = 14$ m. θ_2 is varied in the range 0–90° and ω_1 and ω_2 computed at 10° intervals.

For case (C2) of Figure 4 with smaller overhang, $g_2 = 1$ m and $I_{02} = 47\,500$ kg m^2, ω_1 and ω_2 are similarly evaluated for values of θ_2, but for practical reasons θ_2 may not be able to approach 0° in order to avoid contact with the beam. The natural frequencies are given in Table 2.

4. MODE SHAPES

The natural frequency ω_n is inserted in equation (9), where all the matrix elements are now known. Letting, for example, $A = 1$ and deleting any one of the four equations (10), the remaining three equations can be solved for B, C and D.

Thus, knowing all the variables d_{ij}, A, B, C and D are inserted into equation (2), with the known ω_n, which yields the nth mode shape $y_n(x)$. Figure 5 shows $y_n(x)$ for ω_1 and ω_2 as listed in Table 2 for configuration (C1) with $\theta_2 = 0°$.

To illustrate the effect of unequal or symmetric and asymmetric masses on the mode shapes consider Figure 6 which shows a symmetric mass system.

The properties are $M_1 = M_2 = 10^4$ kg, $I_{01} = I_{02} = 6 \times 10^4$ kg m^2, $g_1 = g_2 = 1{\cdot}5$ m, $\lambda_1 = \lambda_2 = 10^{15}$ N m/rad, $m_b = 3{\cdot}9786$ kg/m, $EI = 3 \times 10^6$ N m^2, $L = 14$ m, $\theta_1 = \theta_2 = 90°$. Then $\omega_1 = 2{\cdot}669$ rad/s and $\omega_2 = 4{\cdot}902$ rad/s.

The mode shapes corresponding to ω_1 and ω_2 are shown in Figure 7.

Figure 7 shows that in order to achieve force and moment equilibrium in the second mode, the rotation of the two masses in the same direction is counteracted by a rigid-body rotation of the whole system in the opposite direction. This is indicated by the straight dashed line connecting the two beam ends. Note that in the symmetric mass case, this line must pass through the nodal point N.

Now for comparison with Figure 7 take an asymmetric mass system with $M_1, I_{01}, g_1, \lambda_1, \lambda_2, m_b, EI, L, \theta_1$ and θ_2 as above but $M_2 = 5000$ kg, $I_{02} = 8333$ kg m^2, $g_2 = 1$ m. Then $\omega_1 = 3{\cdot}321$ rad/s and $\omega_2 = 10{\cdot}429$ rad/s. The corresponding mode shapes are shown in Figure 8.

In Figure 8 the nodal point N in mode 2, which was at the centre of the undeformed beam axis in the symmetric mass case, has now moved towards the larger mass, as expected. As in Figure 7, the straight dashed line in Figure 8 indicates the rigid-body rotation of the whole system in the second mode to compensate for the rotation of the two masses in the opposite direction.

Finally, it is noted that for further use in dynamic response analyses the mode shapes in their present form are inconvenient, containing trigonometric and hyperbolic functions, thus causing considerable computational burden. It is therefore proposed to use a standard polynomial fit $y(x) = \sum_{n=1}^{N} a_n x^n$ to represent the exact mode shapes. Typical orders for N are found to be 7 or 8 for the first few modes.

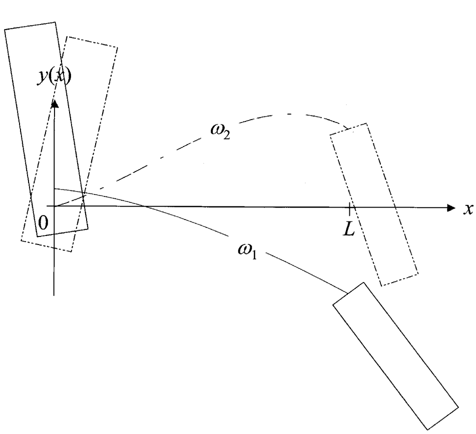

Figure 5. $y_1(x)$ and $y_2(x)$ for C1, $\theta_2 = 0°$.

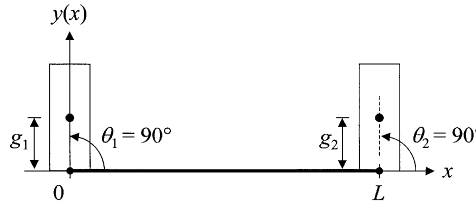

Figure 6. Symmetric system.

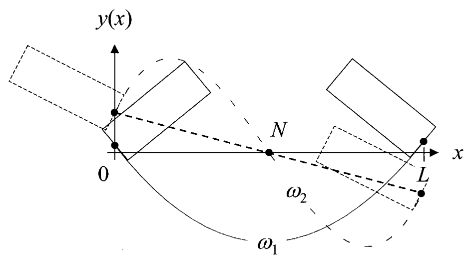

Figure 7. $y_1(x)$ and $y_2(x)$ for symmetric mass system.

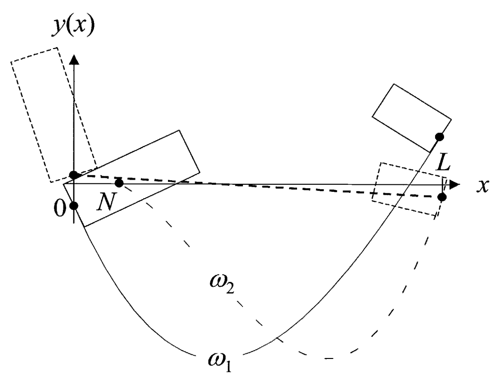

Figure 8. $y_1(x)$ and $y_2(x)$ for asymmetric mass system.

5. ORTHOGONALITY OF NORMAL MODES

The orthogonality condition for a beam with non-zero bending moments and shear forces at $x = 0$ and L has been derived in reference [17]. In the present paper, the bending moments and shear forces are due to the rotational inertias, I_{01} and I_{02}, and the masses M_1 and M_2.

For the system in Figure 1 a hitherto unpublished orthogonality condition is derived and incorporates the shear force and bending moment boundary conditions of equations (5)–(8). The analysis is, however, more involved than [17] due to the presence of torsion springs between the end masses and the beam.

For harmonic motion in mode r, equation (1) becomes

$$EI\, y_r^{\mathrm{iv}}(x) - m_b \omega_r^2\, y_r(x) = 0, \tag{13}$$

which after multiplying by another mode shape $y_s(x)$ and integrating along the beam gives

$$\int_0^L [EI\, y_r^{\mathrm{iv}}(x) - m_b\omega_r^2 y_r(x)]\, y_s(x)\,\mathrm{d}x = 0. \tag{14}$$

Integrating equation (14) by parts gives

$$[EI\, y_r'''(x) y_s(x)]_0^L - \int_0^L EI\, y_r'''(x) y_s'(x)\,\mathrm{d}x - \int_0^L m_b\omega_r^2\, y_r(x)\, y_s(x)\,\mathrm{d}x = 0. \tag{15}$$

A second integration by parts leads to

$$[EI\, y_r'''(x) y_s(x) - EI\, y_r''(x) y_s'(x)]_0^L - \int_0^L EI\, y_r''(x) y_s''(x)\,\mathrm{d}x - \int_0^L m_b\omega_r^2\, y_r(x) y_s(x)\,\mathrm{d}x = 0. \tag{16}$$

Interchanging symbols r and s in equation (16) gives

$$[EI\, y_s'''(x) y_r(x) - EI\, y_s''(x) y_r'(x)]_0^L - \int_0^L EI\, y_s''(x) y_r''(x)\,\mathrm{d}x - \int_0^L m_b\omega_s^2\, y_s(x) y_r(x)\,\mathrm{d}x = 0. \tag{17}$$

Subtracting equation (17) from (16) yields

$$(\omega_s^2 - \omega_r^2)\int_0^L m_b\, y_s(x) y_r(x)\,\mathrm{d}x + [\underset{(a)}{EI\, y_r'''(x) y_s(x)} - \underset{(b)}{EI\, y_s'''(x) y_r(x)} - \underset{(c)}{EI\, y_r''(x) y_s'(x)} + \underset{(d)}{EI\, y_s''(x) y_r'(x)}]_0^L = 0. \tag{18}$$

The terms (a)–(d) in equation (18) are written in terms of the boundary conditions in equations (5)–(8) as follows.

At $x = L$, equations (8) and (18a) give

$$[-M_2\omega_r^2 y_r(L) - g_2 M_2\omega_r^2 (y_r'(L) - \alpha_{2r})\cos\theta_2]\, y_s(L). \tag{19a}$$

From equation (18b)

$$[M_2\omega_s^2 y_s(L) + g_2 M_2\omega_s^2 (y_s'(L) - \alpha_{2s})\cos\theta_2]\, y_r(L). \tag{19b}$$

From equations (18c) and (7)

$$[-I_{02}\omega_r^2 (y_r'(L) - \alpha_{2r}) - g_2 M_2\omega_r^2\, y_r(L)\cos\theta_2]\, y_s'(L). \tag{19c}$$

From equations (18d) and (7)

$$[-I_{02}\omega_s^2(y_s'(L)-\alpha_{2s})+g_2M_2\omega_s^2 y_s(L)\cos\theta_2]\,y_r'(L). \tag{19d}$$

Equation (19c) is now written in the form

$$[-I_{02}\omega_r^2(y_r'(L)-\alpha_{2r})-g_2M_2\omega_r^2 y_r(L)\cos\theta_2][y_s'(L)-\alpha_{2s}+\alpha_{2s}]. \tag{19e}$$

Substituting equation (7) for the first bracketed term in equation (19e) and using equation (4b) for multiplication by α_{2s} in the second bracketed term gives

$$\begin{aligned}&-I_{02}\omega_r^2(y_r'(L)-\alpha_{2r})(y_s'(L)-\alpha_{2s})\\&\quad-g_2M_2\omega_r^2 y_r(L)\cos\theta_2(y_s'(L)-\alpha_{2s})-\lambda_2\alpha_{2r}\alpha_{2s}.\end{aligned} \tag{20a}$$

Similarly, equation (19d) becomes

$$\begin{aligned}&I_{02}\omega_s^2(y_s'(L)-\alpha_{2s})(y_r'(L)-\alpha_{2r}).\\&\quad+g_2M_2\omega_s^2 y_s(L)\cos\theta_2(y_r'(L)-\alpha_{2r})+\lambda_2\alpha_{2r}\alpha_{2s}.\end{aligned} \tag{20b}$$

Finally, adding equations (19a), (19b), (20a) and (20b) and substituting in equation (18) yields

$$\begin{aligned}(\omega_s^2-\omega_r^2)I_{rs}(L)=(\omega_s^2-\omega_r^2)\bigg[&\int_0^L m_b y_r(x)y_s(x)\,\mathrm{d}x+M_2y_r(L)y_s(L)\\&+I_{02}(y_r'(L)-\alpha_{2r})(y_s'(L)-\alpha_{2s})+g_2M_2y_s(L)\cos\theta_2(y_r'(L)-\alpha_{2r})\\&+g_2M_2y_r(L)\cos\theta_2(y_s'(L)-\alpha_{2s})\bigg]=0.\end{aligned} \tag{21}$$

A similar result is obtained by replacing $y_r(L), y_s(L), y_r'(L), y_s'(L), \alpha_{2r}$ and α_{2s} by $y_r(0), y_s(0), y_r'(0), y_s'(0), \alpha_{1r}$ and α_{1s} to give $I_{rs}(0)$. The orthogonality condition for modes r and s is hence

$$I_{rs}(0)+I_{rs}(L)=0 \tag{22}$$

for $r \neq s$. For $r = s$ the generalized mass is given by equation (21) as

$$I_{rr}(0)+I_{rr}(L)=M_r. \tag{23}$$

Equation (1) is reduced to modal form by substituting

$$y(x,t)=\sum_{n=1}^{N} y_n(x)q_n(t) \tag{24}$$

and using equations (22) and (23) [14].

In equation (21) the modal rotations α_{ir} and α_{is} are calculated from equation (4) thus for mode s

$$\alpha_{1s}=\frac{EI\,y_s''(0)}{\lambda_1}\quad\text{and}\quad\alpha_{2s}=\frac{EI\,y_s''(0)}{\lambda_2}, \tag{25}$$

where $y_s''(x)$ is obtained from equation (2) with known values of A–D.

6. CONCLUSIONS

A unique analytical solution is presented for the natural frequencies, mode shapes and orthogonality conditions of a single free–free beam with large off-set masses connected to the ends of the beam by torsion spring restrained revolute joints.

The first two natural frequencies have been determined for a range of fixed end mass orientations and the method has been validated against known results for the first four natural frequencies of a beam without end masses.

The study provides a foundation for the dynamic response analysis of single- and multi-link flexible articulated space robotic systems which are currently being studied by the authors, with application to the Space Shuttle Remote Manipulator and Space Station Mobile Manipulator Systems.

ACKNOWLEDGMENTS

The authors wish to express their thanks to Professor Robin Langley of the Department of Engineering, Cambridge University for his advice in preparing this paper.

REFERENCES

1. Y. Chen and L. Meirovitch 1995 *Journal of Guidance and Control* **18**, 756–766. Control of a flexible space robot executing a docking maneuver.
2. P. A. A. Laura, J. L. Pombo and E. A. Susemihl 1974 *Journal of Sound and Vibration* **37**, 161–168. A note on the vibrations of a clamped–free beam with a mass at the free end.
3. J. Haener 1958 *Journal of Applied Mechanics* **25**, 412. Formulas for the frequencies including higher frequencies of uniform cantilever and free–free beams with additional masses at the ends.
4. B. R. Bhat and H. Wagner 1976 *Journal of Sound and Vibration* **45**, 304–307. Natural frequencies of a uniform cantilever with a tip mass slender in the axial direction.
5. W. E. Baker 1964 *Journal of Applied Mechanics* **31**, 35–37. Vibration frequencies for uniform beams with central masses.
6. R. C. Hibbler 1975 *Journal of Applied Mechanics* **42**, 501–502. Free vibrations of a beam supported by unsymmetrical spring-hinges.
7. K. R. Chun 1972 *Journal of Applied Mechanics* **39**, 1154–1155. Free vibration of a beam with one end spring-hinged and the other free.
8. M. J. Maurizi, R. E. Rossi and J. A. Reyes 1976 *Journal of Sound and Vibration* **48**, 565–568. Vibration frequencies for a uniform beam with one end spring-hinged and subjected to a translational restraint of the other end.
9. T. W. Lee 1973 *Journal of Applied Mechanics* **95**, 813–815. Vibration frequency for a uniform beam with one end spring-hinged and carrying a mass at the other free end.
10. M. S. Hess 1964 *Journal of Applied Mechanics* **31**, 556–558. Vibration frequencies for a uniform beam with central mass and elastic supports.
11. S. H. Farghaly 1992 *Journal of Sound and Vibration* **2**. Bending vibrations of an axially loaded cantilever beam with an elastically mounted end mass of finite length.
12. D. Li, J. W. Zu and A. A. Goldenberg 1998 *Mechanic Machines Theory* **33**, 1031–1044. Dynamic modeling and mode analysis of flexible-link, flexible-joint robots.
13. C. L. Kirk and F. L. Doengi 1994 *ACTA Astronautica* **32**, 561–576. Closed-loop vibration control of a flexible space shuttle manipulator.
14. S. Timoshenko, D. H. Young and W. Weaver Jr 1974 *Vibration Problems in Engineering*. New York: John Wiley and Sons; fourth edition.
15. J. P. Den Hartog 1985 *Mechanical Vibrations*. New York: Dover Publications Inc.
16. D. J. Hedley 1987 *Design Characteristic and Design Feature Analysis of the Shuttle Remote Manipulator Arm*. Society of Automotive Engineers.
17. L. Meirovitch 1986 *Elements of Vibration Analyses*, 221–231. New York: McGraw-Hill Book Company.